IEEE Transactions on Nuclear Science, Vol.NS-25, No.1, February 1978

DESIGN AND PERFORMANCE CHARACTERISTICS OF A PRODUCTION MODEL POSITRON IMAGING SYSTEM

L. R. Carroll

The Cyclotron Corporation
Berkeley, California

ABSTRACT

A simple model is presented which is used to characterize positron-imaging systems employing annihilation coincidence detection. The model is particularly useful in describing sensitivity for true coincidences, vulnerability to accidental coincidences, and overall count-rate capability in systems made of arrays of discrete detectors.

An example is given of a commercially available positron imaging system. A design layout is shown which meets performance goals. Actual system performance is described.

INTRODUCTION

An appreciation of the advantages of positron-emitting isotopes in nuclear medicine has stimulated the development of imaging systems which exploit the unique properties of positron annihilation coincidence detection (ACD). Following the successful application of these techniques at various research institutions, ACD imaging systems are now becoming available commercially. At the Cyclotron Corporation we have produced such a system based on a prototype developed at the Physics Research Laboratory of the Massachussetts General Hospital, (Ref. 1).

ACD systems developed to date fit either of two general categories: Ring detector systems or planar detector systems. Ring systems are presently employed primarily for emission computed tomography, taking one or more "slices" transverse to the axis of the subject under study. Plane detector systems can characterize an extended volume either through multiple transverse section "slices" or through lateral-section tomography.

SYSTEM DESCRIPTION

The Cyclotron Corporation positron imaging system is modeled after "PC II", the second-generation positron camera developed at the Massachussetts General Hospital. The system, which will accommodate any part of the body, employs two planar arrays of NaI(Tl) crystal scintillation detectors. Each array contains 140 crystals, 20 mm diameter by 38 mm long, arranged on a 2.8 cm grid.

In each array the crystals are viewed by a total of 82 photo-multiplier tubes, 3.8 cm dia., through a set of thin light pipes. This sharing arrangement affords a substantial reduction in cost and complexity and is a key feature of the system.

Each crystal in the array is viewed by 2 PMT's and each PMT (except at the edges) looks at four crystals as in Fig. 1. See Reference 1 for a complete description of the sharing scheme.

Each PMT is connected to its own leading-edge timing discriminator. The gain of each PMT is set so that a 511 keV photopeak event gives a 1 mA pulse in 50 ohms. The discriminator trigger level is set at 500 μvolts so as to minimize timing walk due to pulses of varying amplitudes.

To eliminate response to single-photon events related to dark current or resulting from the noisy "tails" of NaI scintillation pulses, the input signal must satisfy an amplitude and time duration criterion before a timing signal will be issued from the discriminator.

In actual use, with a positron-emitting sheet-source placed midway between the detector arrays, the FWHM of the distribution of NaI-NaI response times is 7.5 ns, while the width at the baseline is 20 ns for the entire ensemble of detectors over the entire spectrum of interactions from 50 keV to 511 keV.

The leading-edge signals from the timing discriminators are "OR-ed" together in ten overlapping fields and applied to a set of ten fast-coincidence gates. Whenever a coincidence condition is satisfied, i.e., two 10 ns pulses overlap, an "enable" signal is returned which gates positional data into respective arrays of 82 one-bit registers. See Fig. 2 for a simplified signal flow diagram.

It should be noted, in passing, that the underlying design philosophy in a multi-element ACD system is to maintain sufficient redundancy to insure minimum loss of information due to dead time in the coincidence circuitry or in subsequent circuitry when operating at very high event rates.

Fig. 3 shows a more comprehensive system block diagram. We divide the fast-coincidence circuitry into ten overlapping fields so as to minimize the dead-time for a single event. We impose a spatial criterion for valid coincidence: Each crystal may be in coincidence with any of its 5 x 5 = 25 nearest neighbors.

We refrain from any "packing" of the data up to this point. Validation of data in the spatial domain is performed by the "slow coincidence" circuitry (see Fig. 3) which can reject stray events outside a valid field without having to veto good data.

After validation by the "slow-coincidence" circuitry, the PMT positional signals are sent along to the address and output buffer circuitry. Here the PMT signals are "AND-ed" to create a pair of individual crystal-position identifiers.

The data is examined, in turn, for any remaining multiple-coincidence events which, at this point, must be vetoed. Next the individual crystal-position data is "packed" into a 12 bit crystal-pair indentifier, bufferred, then sent on to the computer interface.

We employ the Gamma 11 nuclear medical computer system by Digital Equipment Corporation. Our data interface emulates the DEC NC-11a normally supplied with the system. The interface provides high-speed direct memory access in histogram or list-mode data

0018-9499/78/0200-0606$00.75

acquisition at up to 180,000 words per second.

In addition, we have provided for computer control of the positron camera detector positioning as required in emission C.T. and high-resolution lateral imaging. Detector rotation and linear scan position are under program control. Detector height, separation, and rotation may be set manually.

IMAGING MODES

Lateral Imaging

Each crystal in a detector array is in coincidence with many crystals in the opposite array. This leads naturally to a facility for plane tomographic imaging. Isotope distributions are detected and displayed on selected focal planes. Activity off the desired focal plane appears blurred.

Since each crystal may be in coincidence with its 25 nearest neighbors there are a total of 2848 possible coincidence pairs (140 x 25 less edge and corner effects). The "rays" between detectors distribute themselves uniformly on four focal planes paralled to the detector faces and spaced at .2, .4, .6 and .8 times the distance between detectors. See Fig. 4.

Because of the discrete sampling, off-plane activity does not necessarily blur uniformly in back projection, but rather may clump and form patterns. This effect can be considerably reduced by moving the detectors in small steps, taking frames of data and reconstructing on the desired plane. This helps to smooth the patterns caused by off-plane activity since in effect, we come closer to satisfying the sampling theorem throughout the subject volume. See Ref. 2 for a discussion of this phenomenon.

A static lateral image is presently made up of five separate frames taken in steps of 0.56 cm, then shifted appropriately and back-projected for display on selected focal planes.

Techniques involving deconvolution of the system transfer function to remove, rather than merely blur, the off-plane activity have been proposed (Ref. 3) for systems employing continuous detectors. Such techniques can be applied to discrete systems such as this, provided the appropriate spatial sampling criteria are met. Methods for removal of off-plane data are presently under study. Such methods have the potential for better quantitative display and, if successful, would more effectively complement the information obtained in transverse-axis computed tomography.

C. T. Imaging

The Cyclotron Corporation positron imaging system has been designed for high-resolution, multi-slice, transverse-axis computed tomography. Up to 23 slices, 1.4 cm FWHM can be acquired in a single study. If desired, images may be reconstructed in thicker sections and/or at less than the finest resolution.

It is of paramount importance in high-resolution emission C.T. that all sampling criteria--both in angular and in linear sampling--be satisfied. To achieve 1 cm FWHM in C.T. reconstruction requires sampling at greater than 2 F_{max} samples per cm. In the data domain (after sampling through finite detector apertures) F_{max} is nominally .9 cm^{-1}.

At this stage of development we find it expedient to oversample: We take data in 29 angular steps. Each step gives five views for a total of 145 angular projections. Each angular projection, in turn, is sampled in 8 steps of 3.5 mm.

Sampling is easily tailored to fit a particular study. Coarser sampling may be used for studies at lower resolution.

After acquisition, the data is separated into "slices". Data from a transmission scan may be used to correct for attenuation in the object. Decay correction and "random" subtraction are performed at this time.

Image reconstruction is done through back-projection of filtered projections: After sorting the data into linear projections each view is convolved with a correction filter derived from the "windowed ramp" in the frequency domain.

We are presently evaluating a family of filter functions of the form:

$$\mathcal{F}(f) = |f| \exp\left[-(f/B)^n\right] \qquad (1)$$

where f = spatial frequency variable
B = selectable bandwidth parameter
n = selectable integer; 4, 6, 8

These functions give high resolution, particularly when compared with more gradual--cutoff filters such as the Hann--weighted ramp (for a given cutoff frequency). Ideally, we try and match the filter characteristic to the data. The shape and bandwidth of the filter function are selected to optimize reconstruction of the object while minimizing the propogation of noise. A recent discussion of this concept is given in Ref. 6.

Back projection is accomplished in a 64 x 64 field and the resulting image is then interpolated to 128 x 128. Subsequent processing and display are done through standard Gamma 11 software supplied by DEC.

PERFORMANCE MODEL FOR ACD SYSTEMS

Sensitivity

The sensitivity of an imaging system should relate to extended sources since, in practical study situations, the radionuclide is always distributed over a volume. A useful measure of sensitivity, following Ref. 4, is the response to an infinite sheet source of activity density σ decays/second-cm^2. This corresponds to the response at "DC" or zero spatial frequency. For a system made up of discrete detectors we can derive an expression for the response of a single detector pair and then sum the contributions of all pairs. Consider the detectors arranged as in Fig. 5.

let a = area of each detector
2R = distance between detectors
σ = activity density-decay/sec-cm^2
η = probability of useful interaction when a photon strikes the detector (including dead-time effects)

For coincidence detection of the collinear annihilation radiation, only activity within the dotted "tube" connecting the detectors will contribute to the true coincidence count rate, r_t. For the situation shown in Fig. 5, for round apertures, it is easily shown that:

$$r_t = \frac{a^2 \eta^2 \sigma}{8\pi R^2} \quad \text{counts/sec} \qquad (2)$$

The sensitivity per pair is given by:

$$k_t = \frac{r_t}{\sigma} = \frac{a^2\eta^2}{8\pi R^2} \quad \frac{\text{counts} \cdot \text{cm}^2}{\text{decay}} \qquad (3)$$

For a system made up of many discrete detector pairs the system sensitivity, \$, is simply the sum of the individual sensitivities:

$$\$ = N\,k_t = \frac{Na^2\eta^2}{8\pi R^2} \quad \frac{\text{counts} \cdot \text{cm}^2}{\text{decay}} \qquad (4)$$

where N = number of detector pairs

This result does not depend substantially on the actual position of the sheet source.

In the present case a = 3.14 cm^2, η = .7, N = 2848, and R is adjustable from 25 to 45 cm. The measured sensitivity in air agrees well with that predicted by Eq. 4 .

When an ACD system is arranged in a ring configuration the DC sensitivity may be calculated on the basis of the response to an annular sheet of density $\sigma/2$ so that each detector pair sees an effective density of σ and equation (4) still holds.

Resolution

The FWHM of the point--or--line spread function gives a measure of the ability of an imaging system to resolve detailed structures. In ACD systems that employ discrete detectors the FWHM is nominally one-half the detector aperture diameter.

In the system under discussion, the detector apertures are 2 cm, giving an intrinsic resolution of less than 1 cm FWHM. For C.T. reconstruction the sampling and reconstruction bandwidth also effect the final image. Fig. 6 compares the fidelity of the system for lateral and C.T. imaging. The line sources are 1 mm I.D. plastic tubing filled with ^{22}Na and spaced 2.5 cm in air. Each image contains approximately 1 million counts.

A complete description of imaging system performance requires consideration of the total point spread function (PSF) or equivalently, the modulation transfer function (MTF). Other components, beside the true coincidence response, are scatter and accidental coincidences, which add "tails" to the PSF.

The "delayed coincidence" technique affords an accurate estimate of the number of randoms in any region of the image. The effects of scatter are more difficult to evaluate. Techniques involving pulse-height analysis are less effective with 511-keV annihilation radiation than with low-energy single-photon imaging (Ref. 5), since scatter in the subject is predominantly low-angle and the energy lost in such interactions is too low to permit effective energy discrimination at the detector.

Effective system shielding is essential in reducing the response to scatter and randoms. We employ a special iris "collimator" which limits the field of view for each crystal so as to control the response to single events. The use of lead scatter filters in front of the detectors is of some value in reducing the singles response. However, we have found the marginal improvement obtained with scatter filters to be substantially less than that reported in Ref. 7, since we already limit the field of view. Our results are in general agreement with Ref. 5.

We do observe that the filter function used in C.T. reconstruction helps significantly in reducing the low-frequency scatter and random contribution in the final image. Figure 7, for example, shows a set of 2.8 cm cross-sectional slices taken through a scattering medium; a gallon jug (16 cm dia.) filled with water and dissolved ^{13}N. A 2.5 cm dia. lucite rod "cold spot" rests inside.

Each section image contains approximately 1,200,000 counts. Decay correction and attenuation correction (utilizing knowledge of the shape and density of the object) were applied to the image data.

Sensitivity Versus Resolution

There is no difficulty in concept in comparing systems that have the same resolution if one has higher sensitivity, or vice versa. In general the situation is more complicated: To compare systems when one has higher sensitivity but poorer resolution than the other.

In positron ACD systems made of discrete detectors the resolution and sensitivity are governed by the size of the detector apertures. It is generally the case that if the resolution is extremely fine, the sensitivity is too low to give sufficient counts to resolve adjacent regions statistically. If the sensitivity is very high, the resolution may be very poor so that adjacent regions cannot be resolved spatially. Practical results are obtained between these extremes.

Beck (Ref. 4) suggests a figure of merit, Q, which tells us how well we can resolve objects of frequency component f in the presence of statistical uncertainty:

$$Q(f) = \$ \left[MTF\ (f)\right]^2 \qquad (5)$$

Suppose we have an ACD system with adjustable apertures. Figure 8 shows a comparison of Q(f) for FWHM resolution of 1. and 1.4 cm respectively. Here it is assumed that the spread function is Gaussian, where r = FWHM resolution:

$$PSF(x) = \exp(-\pi X^2/r^2) \qquad (6)$$

The MTF is also Gaussian (Ref. 8)

$$MTF(f) = \exp(-\pi r^2 f^2) \qquad (7)$$

The D.C. sensitivity of the 1.4 cm system is obviously much higher, in accordance with Eq. (3). However, the resolution of spatial detail beyond .5 cm^{-1} requires substantially less data (fewer counts) in the system with higher resolution.

This effect is particularly important in emission C.T. where the frequencies in the object space may be low enough, i.e., objects widely separated--but, the frequencies in the data space will always be higher since the data is in the form of projections or shadows.

Figure 9 shows a study inspired by Ref. 9. The image contains 200,000 counts and was reconstructed using the filter of equation (1) for n = 6 at 1.0 cm^{-1} cutoff frequency. (B=.707).

The points (2 mm dia.) in the horizontal row are separated by 2 cm. The intensity profile confirms the high resolution in C.T. imaging.

Count Rate Capability

In large-scale ACD systems an ultimate limit to performance is imposed by a constraint on allowable count rate. The number of true coincidences is only a small fraction of the single events. High single event rates cause system dead-time which, in turn, reduces overall efficiency. Single events also give rise to accidental coincidences as a consequence of finite resolving time. The rate of accidental coincidences for a single detector pair is approximated by:

$$r_r = 2\tau_r \mathcal{N}_s^2 \qquad (8)$$

where τ_r = coincidence window
$\mathcal{N}_s$ = singles rate per crystal
= $K_s\sigma$

The sensitivity of a single crystal to single events, ks, is a function of detector area, efficiency, and shield aperture. A formula for this sensitivity is derived in the appendix.

The rate of accidental coincidences can be estimated through the "delayed coincidence" technique. This estimate can be subtracted from the total to yield an estimate of the true coincidences. The noise contribution of the accidentals is therefore a consequence of the error in the estimate of the accidentals.

Satisfactory performance may be technically possible even at very high accidental rates, but, as will be shown presently, practical considerations dictate that the accidental rate should not be substantially more than 50% of the total coincidence count rate.

We define a "D.C." signal-to-noise ratio in the image as the mean true counts divided by the standard deviation of trues plus randoms. We have (expressed per detector pair):

$$\mathcal{R} = \frac{n_t}{\sqrt{n_t + 2n_r}} \qquad (9)$$

where $n_t = \mathcal{S} k_t \sigma t$ = true counts per detector pair (10)

$n_r = 2\tau_r K_S^2 \sigma^2$ = random counts per detector pair (11)

and t = integration time
k_t-found from Eq. 3
k_S-from the appendix
$\mathcal{S}$ = unscattered component = .2

Here we are assuming that scatter reduces the true count rate but not the singles rate since relatively few photons are completely absorbed in the object. The choice of $\mathcal{S}$ = .2 for this model is somewhat arbitrary. See Ref. 5 for a proper discussion of scatter geometry.

we have from (9), (10), (11)

$$\mathcal{R} = \frac{k_t \mathcal{S} \sigma \sqrt{t}}{\sqrt{k_t \sigma \mathcal{S} + 4\tau_r k_s^2 \sigma^2}} \qquad (12)$$

for low count rates (see Fig. 10A)

$$\mathcal{R}_o = \sqrt{k_t \mathcal{S} \sigma t} \qquad (13)$$

At low count rates (assuming fixed integration time) $\mathcal{R}$ increases as $\sqrt{\sigma}$ as we would expect. For very high activity levels, where $4\tau_r k_s^2 \sigma^2 \gg k_t \sigma$ (ignoring dead-time) the value of $\mathcal{R}$ approaches:

$$\mathcal{R}_\infty = \frac{k_t}{k_s \cdot 2 \cdot} \frac{\mathcal{S}\sqrt{t}}{\sqrt{\tau_r}} \qquad (14)$$

In Fig.10B we have plotted Eq. (12) as a function of σ for $\mathcal{S}$ = .2 and a detector spacing, 2R, = 60 cm.

Dead Time Effects

In a practical system we cannot reach $\mathcal{R}_\infty$ because of count loss due to dead-time. The dominant loss factor in this system is detector dead-time. A single event will paralyze two photo-multiplier tubes for 600 ns. Two photomultiplier tubes relate to seven crystals (see Fig. 1) so that the probability that a given crystal is not paralyzed is given by:

$$P = \exp\left(-\cdot 7 \times 600 \times 10^{-9} \times \mathcal{R}s \right) \qquad (15)$$

where $\mathcal{R}s$ is the singles rate per crystal--here assumed to be uniform throughout the system.

Subsequent circuitry will, to some extent, also contribute to dead-time. In any system of this sort one must balance complexity against performance to achieve a design goal. In the present case we would be satisfied if it can be demonstrated that the limit to performance occurs at or beyond what would be considered a safe activity concentration in the subject under study.

It is possible, given a source distribution, scatter fraction, detector spacing, etc., to calculate a total dead (or live) time as a function of activity level.

A summary of such a calculation is shown in Fig. 11. It should be emphasized that this result relates to a specific study configuration; in this case we have assumed a uniform sheet source, 60 cm detector spacing, 20% unscattered events, and standard iris shield.

Dead-time reduces efficiency which, in turn, is reflected in the signal-to-noise ratio in the image. The system "live" fraction can be factored into Eqs. (3) and (12). Thus we can determine the behavior of $\mathcal{R}$ at high count rates as shown in curve C in Fig. 10. For the given study and system configuration we observe that it is of little benefit to increase isotope concentration beyond the point where $\mathcal{R}$ actually declines with increasing activity.

In the present example, referring to Fig. 10, the turnover occurs at approximately 10 millicuries in the field of view for a uniform distribution in a scattering medium.

This is consistent with our requirement for performance at and beyond maximum doses likely to be administered to patients.

CONCLUSION

All positron ACD systems share certain performance advantages and also certain limitations. ACD systems which employ discrete detectors are somewhat easier to characterize than are continuous detector systems, though the same principles apply to all. It should be possible to calculate a functional (regional) equivalent to k_t and k_S for continuous detector systems. A knowledge of resolving time and system dead-time should yield estimates of output count rate and signal-to-noise ratio as functions of activity concentration.

As clinical experience is gained in the use of positron-emitting radioisotopes it will become essential to characterize and to compare systems as they relate to specific applications.

We have given some preliminary results obtained during factory start-up of a commercial positron camera. We have shown a simple model for sensitivity, resolution, and count rate capability which places any such system in appropriate perspective.

ACKNOWLEDGEMENT

I wish to acknowledge the essential and timely contribution of Professor Gordon Brownell, Charles Burnham, and co-workers at the Physics Research Laboratory of the Massachussetts General Hospital, in the development of this product.

REFERENCES

1) Brownell, G. L., and Burnham, C. A. Recent Developments In Positron Scintigraphy In Instrumentation In Nuclear Medicine, vol. 2. Hine, G. J. and Sorenson, J. A., Editors, Academic Press , New York, 1974.

2) Brownell, G. L., and Burnham, C. A. MGH Positron Camera, Chapter 14 in Tomographic Imaging In Nuclear Medicine, G. S. Freedman, editor Society of Nuclear Medicine, New York, 1973.

3) Chu, G. and Tam, K. C. Three-dimensional Imaging In The Positron Camera Using Fourier Techniques, Physics in Medicine and Biology, volume 22, number 2, March, 1977.

4) Beck, R. N., Instrumentation and Portrayal of Information, Chapter 2 in Clinical Scintillation Scanning, Freeman, L. M., Johnson, P. M., editors Harper & Row, New York, 1969.

5) Derenzo, S. E., Budinger, T. F., et al High Resolution Computed Tomography of Positron Emitters, IEEE Transactions on Nuclear Science, vol NS-24 No. 1, February, 1977.

6) Cho, Z. H., Burger, J. R., Construction, Restoration, and Enhancement of 2-and 3-Dimensional Images, IEEE Transactions on Nuclear Science vol NS-24, No. 2, April, 1977.

7) Muehllehner, G., et al, Performance Parameters of a Positron Imaging Camera, IEEE Transactions on Nuclear Science, vol NS-23, No. 1, Feb, 1976

8) Bracewell, R. N., The Fourier Transform And Its Applications, Chapter 6, McGraw Hill, 1965

9) Hoffman, E. J., Phelps, M. E., et al, Design And Performance Characteristics Of A Whole-Body Positron Transaxial Tomography., Journal of Nuclear Medicine, 17:493-502, June, 1976.

APPENDIX

Sensitivity of a single detector to single events:

FOR ROUND APERTURES

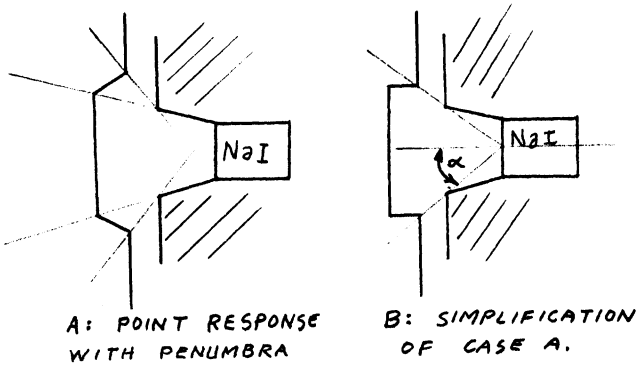

A: POINT RESPONSE WITH PENUMBRA

B: SIMPLIFICATION OF CASE A.

1. Assume that point response for single detector can be characterized by "B" above; that penumbra effects can be summarized by the half-angle α.

2. For a sheet source at distance R we have:

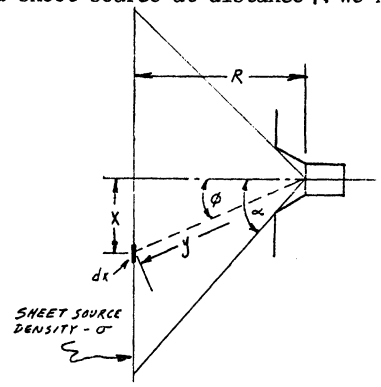

G = response to singles

a = detector area

α = 1/2 angle of aperture

η = detector efficiency

σ = source density decay/sec·cm^2

3. let $dq = 2\pi\sigma x\,dx$

$x = R\tan\phi$

$dx = \dfrac{R\,d\phi}{\cos^2\phi}$

$dG = \dfrac{a\eta\,dq}{2\pi y^2}$

$y = \dfrac{R}{\cos\phi}$

$dG = a\eta\sigma\tan\phi\,d\phi$

$G = a\eta\sigma\int_0^{\alpha}\tan\phi\,d\phi$

$= a\eta\sigma(-\ln\cos\alpha)$

THUS: $K_S = \dfrac{G}{\sigma} = -a\eta\ln\cos\alpha$

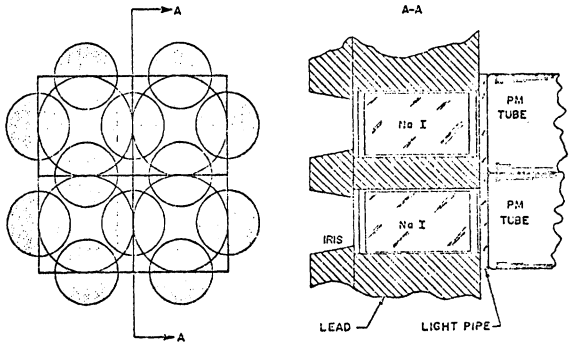

Fig. 1) Sharing of crystals and photomultiplier tubes.

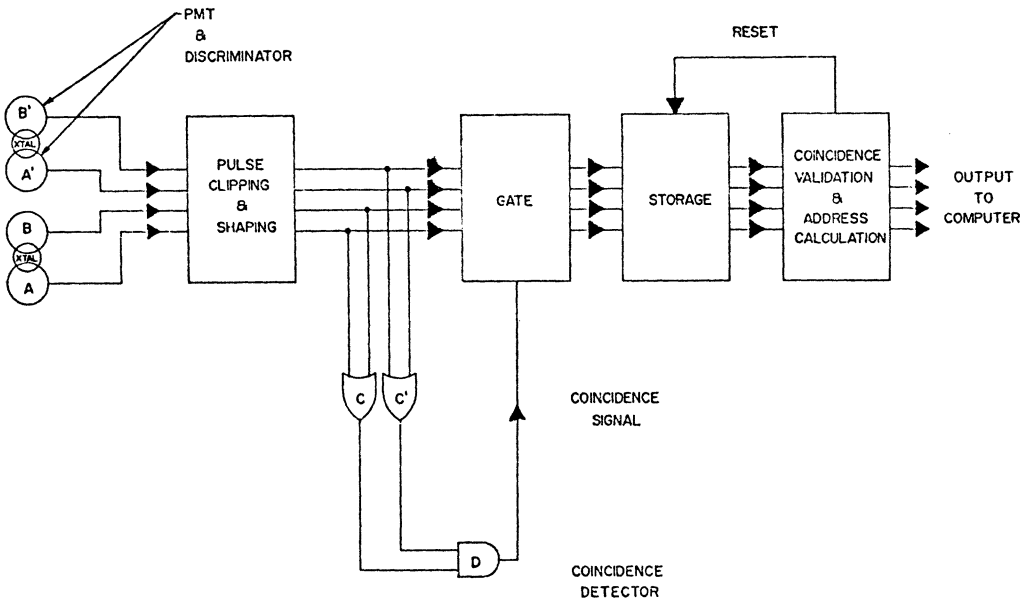

Fig.2. Simplified Signal Flow.

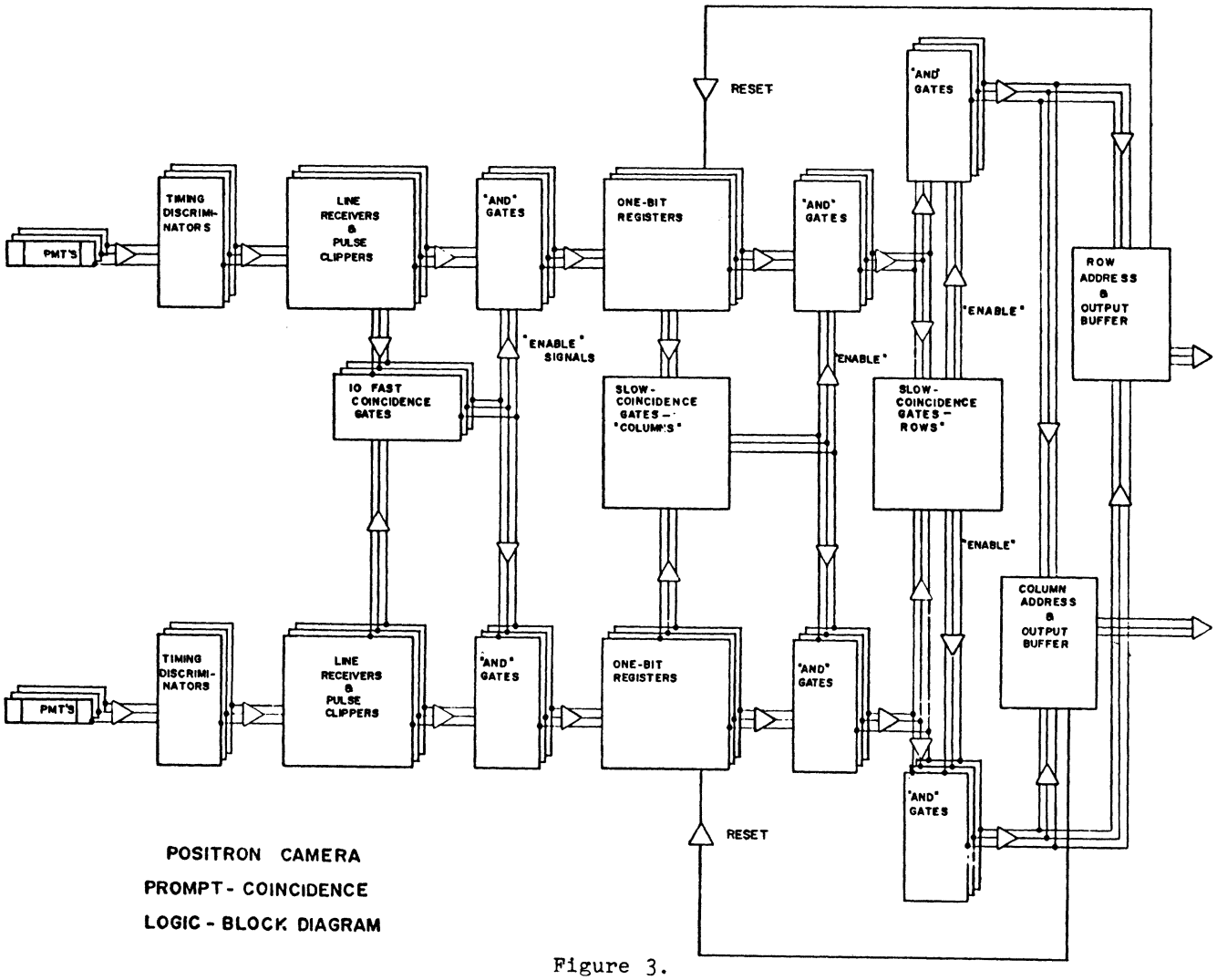

Figure 3.

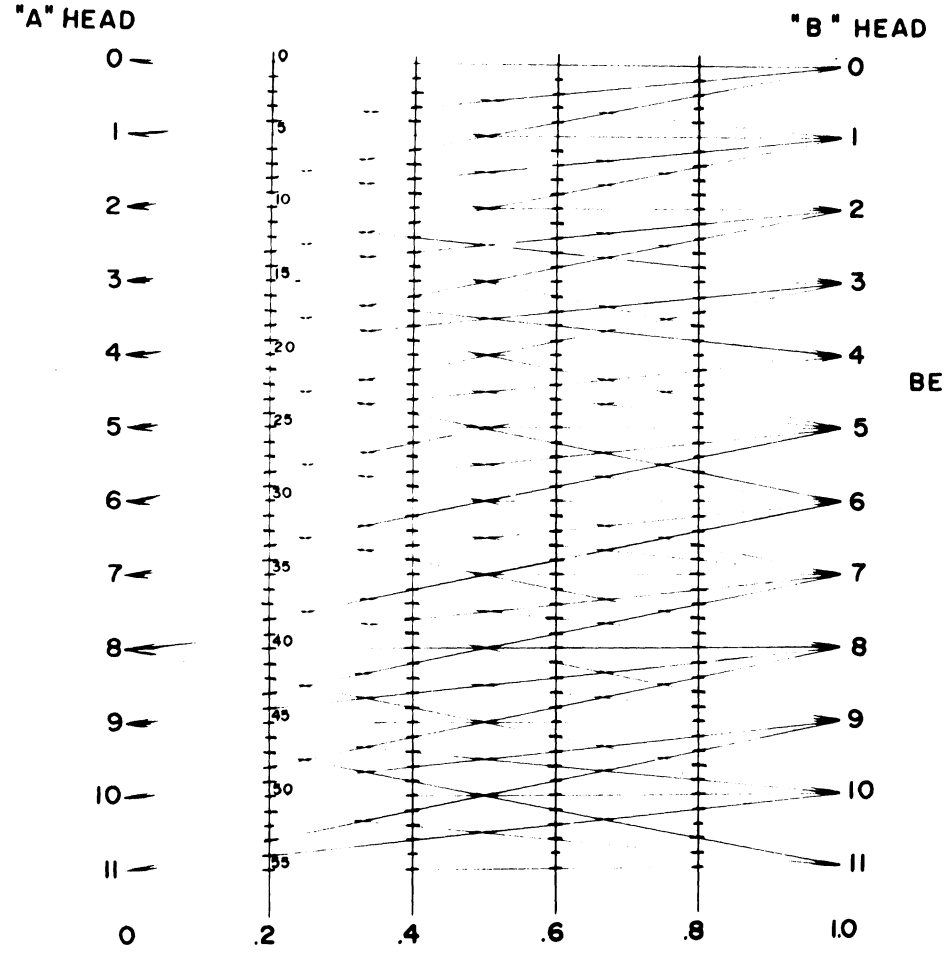

Figure 4.

SHIFTING "PIXELS" BETWEEN FOCAL PLANES:

$P_{(.2)} = 4A + B$

$P_{(.4)} = 3A + 2B$

$P_{(.6)} = 2A + 3B$

$P_{(.8)} = A + 4B$

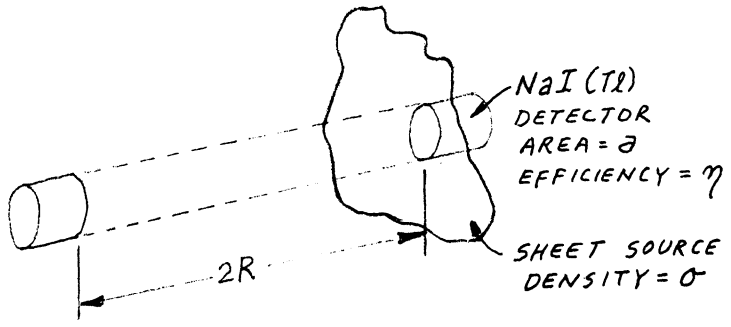

Fig. 5) Basic positron ACD pair.

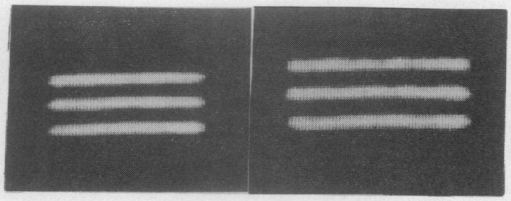

Fig. 6)

Adequate sampling and bandwidth in the reconstruction algorithm insure good fidelity in C.T. imaging. Left: Lateral imaging-line sources (1mm I.D. plastic tubing filled with ^{22}Na) spaced 2.5 cm in air, parallel to detector faces. Right: Same object imaged in a plane transverse to axis of detector rotation.

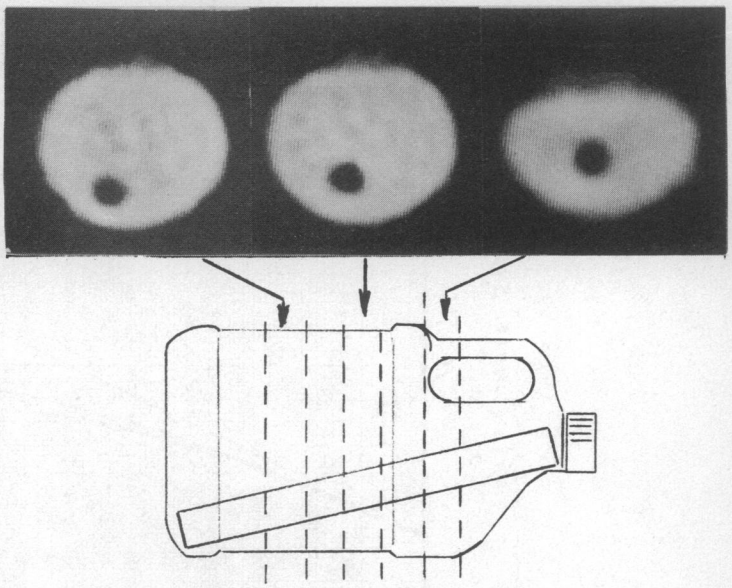

Fig. 7) Coldspot imaging: Study demonstrates the capability of emission C.T. in delineating a cold "lesion" in pool of high activity. Object is a 2.5 cm dia lucite rod in a gallon jug filled with water and dissolved ^{13}N. All images were obtained in a single study; each section contains approximately 1.2 million counts.

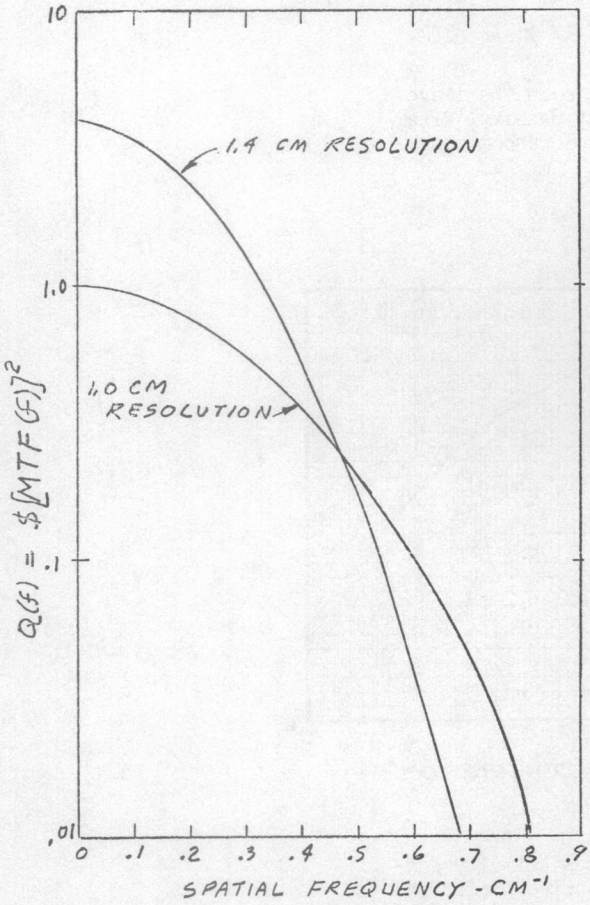

Fig. 8) Figure of merit Q(f) demonstrates trade-off between sensitivity and resolution in ACD systems using discrete detectors.

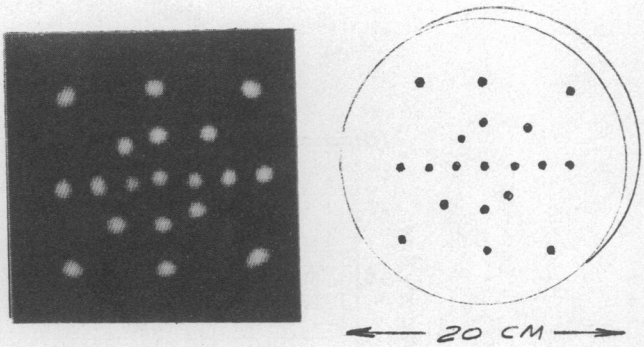

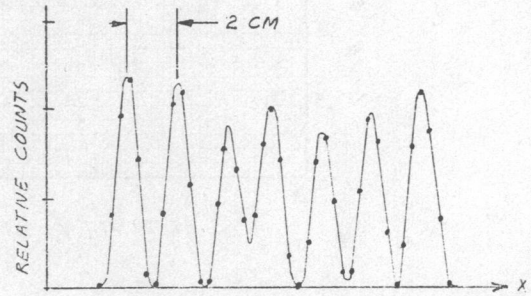

Fig. 9) Point response in C.T. imaging. Objects are 2 mm dia copper wires, containing ^{64}Cu, embedded in plastic disc 20 cm dia and 5 cm thick. Objects are spaced 2, 3, 4, and 5 cm. Image contains 200,000 counts. Below: Intensity profile through row spaced at 2.0 cm.

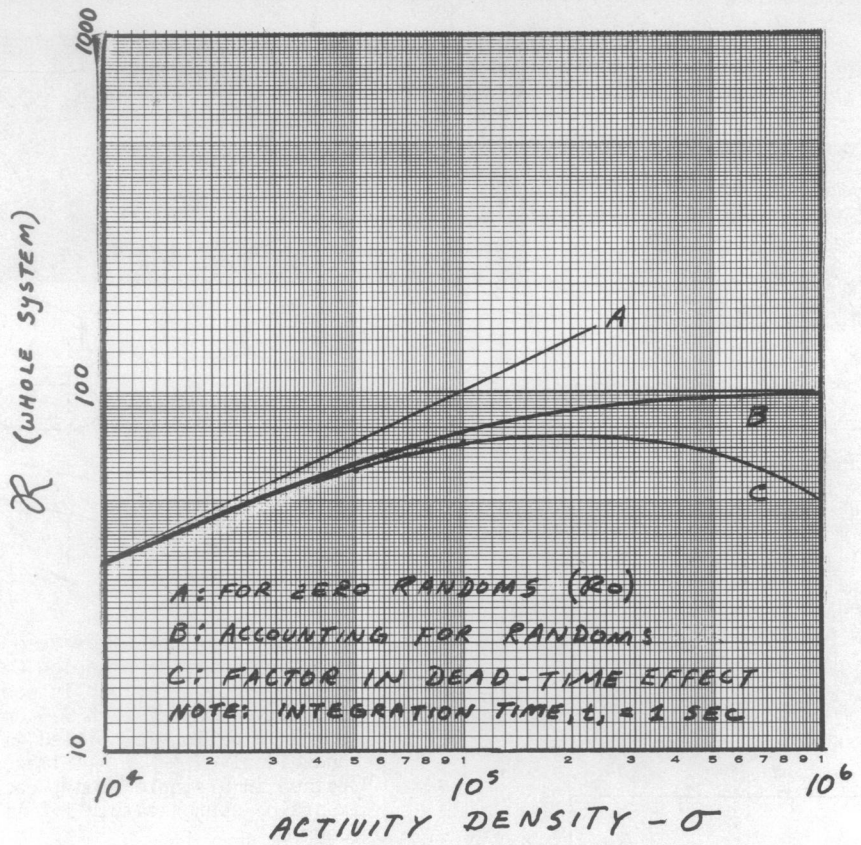

Fig. 10) "D.C." signal-to-noise ratio in the image as a function of activity density, after subtracting an estimate of random contribution.

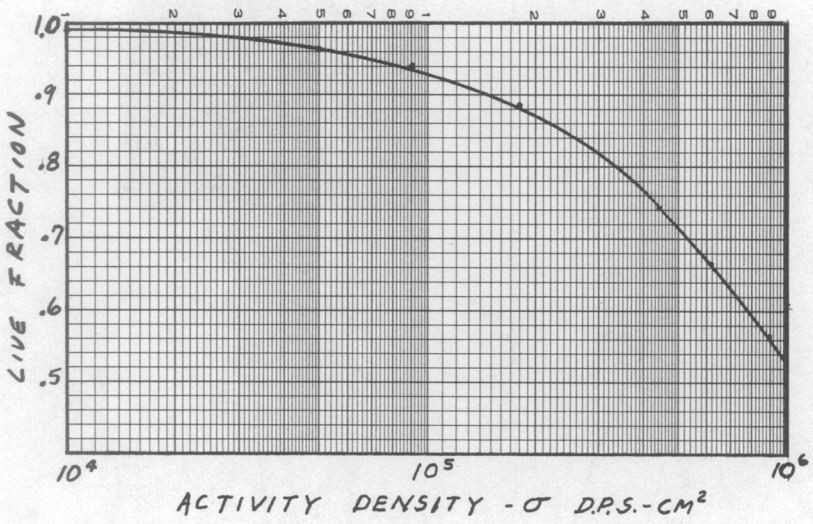

Fig. 11) System "live" time versus activity density in a large sheet source, referred to single channel.